Atmos. Chem. Phys. Discuss., 5, 11911–11928, 2005
www.atmos-chem-phys.org/acpd/5/11911/
SRef-ID: 1680-7375/acpd/2005-5-11911
European Geosciences Union

Atmospheric Chemistry and Physics Discussions

The time-space exchangeability of satellite retrieved relations between cloud top temperature and particle effective radius

I. M. Lensky[1] **and D. Rosenfeld**[2]

[1]Department of Geography and Environmental Studies, Bar-Ilan University, Ramat-Gan, Israel
[2]Institute of Earth Sciences, The Hebrew University of Jerusalem, Jerusalem, Israel

Received: 30 August 2005 – Accepted: 21 October 2005 – Published: 22 November 2005

Correspondence to: I. M. Lensky (lenskyi@mail.biu.ac.il)

Abstract

A 3-min 3-km rapid scan of the METEOSAT Second Generation geostationary satellite over southern Africa was applied to tracking the evolution of cloud top temperature (T) and particle effective radius (r_e) of convective elements. The evolution of T-r_e relations showed little dependence on time, leaving re to depend almost exclusively on T. Furthermore, cloud elements that fully grew to large cumulonimbus stature had the same T-r_e relations as other clouds in the same area with limited development that decayed without ever becoming a cumulonimbus. Therefore, a snap shot of T-r_e relations over a cloud field provides the same relations as composed from tracking the time evolution of T and r_e of individual clouds, and then compositing them. This is the essence of exchangeability of time and space scales, i.e., ergodicity, of the T-r_e relations for convective clouds. This property has allowed inference of the microphysical evolution of convective clouds with a snap shot from a polar orbiter. The fundamental causes for the ergodicity are suggested to be the observed stability of r_e for a given height above cloud base in a convective cloud, and the constant renewal of growing cloud tops with cloud bubbles that replace the cloud tops with fresh cloud matter from below.

1. Introduction

Rosenfeld and Lensky (1998) introduced a technique that was used to gain insights into precipitation forming processes. This technique was applied to AVHRR data, and later to other polar orbiting sensors (VIRS on TRMM, GLI on ADEOS II, MODIS on Terra and Aqua). The Rosenfeld Lensky Technique (RLT) was used in many studies to assess the impact of different aerosols on clouds and precipitation. (Rosenfeld, 1999, 2000; Rosenfeld et al., 2001, 2002, 2004; Rosenfeld and Woodley, 2001, 2003; Ramanathan et al., 2001; Rudich et al., 2002, 2003; Tupper et al., 2004; Williams et al., 2002; Woodley et al., 2000).

The RLT is based on two assumptions:

ACPD

5, 11911–11928, 2005

– The evolution of cloud top effective radius (r_e) with height (or cloud top temperature, T), observed by the satellite at a given time (snapshot) for a cloud ensemble over an area, is similar to the T-r_e time evolution of a given cloud at one location. This is the ergodicity assumption, which means exchangeability between the time and space domains.

– The r_e near cloud top is similar to that well within the cloud at the same height as long as precipitation does not fall through that cloud volume.

The second assumption was verified using in situ aircraft measurements (Rosenfeld and Lensky, 1998; Freud et al., 2005). This paper intends to test the ergodicity assumption using a rapid scan sequence taken by the Spinning Enhanced Visible and Infrared Imager (SEVIRI) on the European METEOSAT Second Generation (MSG) geostationary satellite. To this end, rapid scan data of convective clouds over Africa is used. This paper does not intend to focus on the reasons of the different apparent behavior of clouds in different areas or to associate it with aerosols, but rather to characterize systematic distinct behavior of clouds in different areas, and to show that different clouds in the same area have similar behavior and is steady with time.

2. The data

Data from the Spinning Enhanced Visible and Infrared Imager (SEVIRI) on the European METEOSAT Second Generation (MSG) geostationary satellite (Schmetz et al., 2002) is used in this study. Rapid scan data (three minutes interval, from 10:01 to 15:01 GMT) from 15 December 2003 is used to monitor convective clouds over Africa, during the pre-commissioning phase of the satellite.

Counts from the Native format data files were transformed to radiances and then to reflectances and temperatures at the solar and emissive channels respectively. The solar reflectance component of channel 4 (3.9 μm) was calculated. For the retrieval of the cloud top effective particle size, a look up table (LUT) with entries for the satellite zenith

ACPD
5, 11911–11928, 2005

angle, solar zenith angle, and relative azimuth was used. The LUT was calculated using SSCR (Signal Simulator for Cloud Retrieval) radiative transfer code (Nakajima and King, 1992; Nakajima, 1995) for optically thick clouds such that the surface effects can be neglected at 3.9 μm (Rosenfeld et al., 2004). To make sure that only optically thick clouds are assigned an effective radius a cloud mask was used.

The cloud mask for the retrieval of r_e consists of four steps:

- Minimum reflectance threshold of 50% at the 0.6 μm channel;
- Maximum 10.8 μm brightness temperature ($T_{10.8}$) threshold of 290 K;
- Three intervals of brightness temperature difference between the 10.8 and 12.0 μm channels. The first interval of −0.5 to 1.5 K was applied to pixels with $T_{10.8}$>260 K. The second interval of −0.5 to 1.0 K was applied to pixels with 260>$T_{10.8}$>250 K. The third interval of −0.2 to 1.5 K was applied to pixels with $T_{10.8}$<250 K (see Fig. 1).
- An interval of brightness temperature difference between the 10.8 μm channel and the 8.7 μm channel of −1 to 5 K.

3. Methodology

A chain of programs was applied to the MSG raw data. In the first stage pixel data ($T_{10.8}$ and r_e) from predefined areas of interest (Fig. 2) were saved for the whole data set for further analyses. In the second stage, individual cloud cells (or convective towers) were tracked. To this end we looked for local minimum of $T_{10.8}$ in a running box of 5 by 5 pixels. The cells in each area in each time step were listed in a table. These tables included the cells' location (line, pixel), $T_{10.8}$, and r_e of the coldest pixel (cell center). The coldest (highest) pixel was selected to avoid shadows from neighboring clouds. These shadows reduce the 3.9 μm solar reflectance, and erroneously enlarge the effective radius. In the third stage a cloud-tracking program was applied to track the

ACPD
5, 11911–11928, 2005

individual cells with time and to give them an ID. The tracking routine looks for the shift of the cell center between the time steps. A maximum shift of two pixels per time step was permitted. The two pixels shift enables the tracked cell to shift to a new adjacent bubble of the same cloud. This is done to allow for long enough sequences so the time evolution of the T-r_e plots of the individual clouds can be compared to those of a cloud cluster composed of many clouds at different stages in their life. Finally the classical T-r_e plots of the RLT for the predefined areas in Fig. 2 were saved for all the time steps.

4. Results

4.1. Time-space composition of T-r_e relations

About 150 000 instantaneous convective cells were tracked in the 8 windows in three-minute interval between 10:01 GMT to 15:01 GMT. Figure 3 shows the classical RLT T-r_e plots of areas 2, 3 and 4 at 13:01 GMT. The effective radius of the shallowest clouds in areas 2 and 3 is very small (r_e=5 μm), revealing that the clouds are microphysically continental. The effective radius of cloud droplets in these clouds pass the 15 μm threshold for precipitation (Lensky and Rosenfeld, 1997) only when the clouds develop to heights where $T_{10.8}$<−12°C. On the other hand, the effective radius of the shallowest clouds in area 4 is much larger (r_e=13 μm), and it passes the 15 μm threshold for precipitation at $T_{10.8}$=+5°C. The T-r_e plots of the other areas shows that areas 2, 3, 6 and 8 are microphysically continental, area 4 is microphysically maritime, and areas 5 and 7 are transition between maritime and continental.

The T-r_e plots are formed by calculating the median and other percentiles of the r_e for each 1°C interval of T. The lower/higher percentiles represent the younger/older elements at that height. In Fig. 4 we show T-r_e plots of the 15 percentile of the same areas as in Fig. 3 at one hour intervals: 11:00, 12:00, 13:00 and 14:00 GMT. The 15 percentile was chosen so that the plot will represent the beginning of each microphysical process in the cloud. For example, looking at the line of r_e=15 μm in Fig. 4 will

ACPD
5, 11911–11928, 2005

show the T of onset of precipitation in each plot, or T at which r_e reaches the saturation value of 40 μm indicates that glaciation dominates the cloud from this isotherm and above. It is evident from this figure that the distinct behavior of the clouds in the predefined areas is stable with time. However, there is a small trend of a decrease of the effective radius with time in most of the areas. This may be due to increased vigor of the convection with time from morning to the afternoon, together with the increasing of cloud base height and temperature, all slowing the growth of the r_e with height thus contributing to increased microphysical continentality of clouds during the day. This is manifested by the shift to the left (smaller r_e) of the T-r_e plots.

4.2. The T-r_e time evolution of individually tracked clouds

Convective cloud development can be viewed as consecutive towers that dissipate or merge with previous cloud elements, and new towers replace them and develop some more, and so on until a fully-grown Cb cluster is formed in some cases, or in other cases the clouds dissipate before reaching that stature. The approach that was taken for the cloud tracking was to look for local minima of the temperature field in the cloudy pixels in each time step, and then to track these local minima from one time step to the next based on the cell location (line and column). Tracking the cloud elements results therefore in few long tracks along with many shorter ones that merged into the longest that made it all the way to the mature stage. It is analogous to a river (the long-tracked main cell) with many tributaries (the cells that merge to the primary one), but only one water way connects the initial development to the outlet of the river to the sea (the anvil of the mature storm). Figure 5 shows the time evolution of T and r_e of these longest cloud tracks.

The cells were found to be very often regenerating in the same location, such that after a developing stage (decreasing T and increasing r_e), came a drop in the r_e and rise of the T followed by another developing stage. For example, cell 708 in area 4 of Fig. 5 seems to glaciate after about 60 min (r_e=40 μm) but after about 10 min r_e drops to 27 μm and T increases by 20°C. Maturation of the older glaciated cell segment may

ACPD
5, 11911–11928, 2005

lead to thinning of the segment due to precipitation and evaporation. The resultant increase of the BTD between the 10.8 and 12.0 μm channels causes these pixels to be rejected from the cloud mask. In such case the cell track jumps to adjacent pixels that did pass the criteria of the cloud mask. Other cases like the peaks in the first 40 min of cell 708 represent regeneration of the convective bubbles that form the cloud. These succeeding developing stages follow the general T-r_e characteristics of the area as can be seen in Fig. 5. It follows that the general characteristic T-r_e plot of the area is built upon many regenerating cells that follow the same T-r_e relations (confirming again the second assumption of the RLT).

The dynamic behaviors of single clouds were often very different; still their microphysical behavior remained consistent with the typical T-r_e plot of that area. For example, note in Fig. 5 that cells number 823, 2219 and 2497 that do not make it to Cb (lowest $T>\sim-20^{\circ}$C) have the same r_e for the same T as clouds that become eventually fully grown as cells number 29 and 708 ($T_{29}=-50^{\circ}$C, $T_{708}=-60^{\circ}$C), in spite of the dynamical differences that determined such different fates for these two groups of cells.

The rapid scan of the clouds microstructure allows for the first time to add the time dimension to the microphysics of clouds from space observations. The longevity of highly supercooled (i.e., $T<-10^{\circ}$C) clouds tracked in Fig. 5 is 3–4 times longer than the 10 to 15 min that were previously reported by observations made by repeated aircraft penetrations into tropical and subtropical microphysically continental clouds (Rosenfeld and Woodley, 1997). Also the inferred updraft velocity is smaller than observations. For example, in area 2, it took about 40 min for cells number 4 and 37 to reach the $r_e=15\,\mu$m threshold (at $T=-10^{\circ}$C). This corresponds to very low updraft of about 1.2 ms^{-1}, whereas updrafts >5 ms^{-1} were usually observed by aircraft in situ measurements (Rosenfeld and Woodley, 1997). The discrepancy between the aircraft and satellite observations can be resolved by the suggestion that the tracked cloud top is renewed frequently by new growing cloud bubbles, and the longevity of the supercooled cloud water is a lot shorter than the outline of the cloud top. Furthermore, the effects of cloud drop coalescence to increase r_e and evaporation to decrease r_e nearly cancel

ACPD
5, 11911–11928, 2005

each other and cause further stability of the r_e as long as the cloud is not appreciably glaciated (Freud et al., 2005). The process of the cloud top renewal by sequence of bubbles along with the stability of r_e to maturation of cloud drop distribution at a given T explain the apparent lack of sensitivity of r_e to the elapsing time within the convective cloud life cycle. The lack of time dependence of r_e on T leaves r_e in convective elements almost exclusively as a function of T. This is the fundamental cause for the exchangeability of time and space, or the ergodicity of the T-r_e relations.

4.3. Comparing time and space dimensions

Tracking the cells and then composite back their elements can provide further supporting evidence. This is done in Fig. 6, which shows similar T-r_e relations for cells of vastly different time evolution in Fig. 5. For example, cell number 4 of Fig. 5 continued to develop for another 20 min, reaching $T=-20^{\circ}$C and $r_e=27\,\mu$m, but then started to decay, and vanished after another 20 min. Cell number 37 continued growing, starting to glaciate at $T<-20^{\circ}$C after about 70 min, about 50 min after crossing the 0°C isotherm, and vanished only after 110 min. When plotting on Fig. 6 the T-r_e relations of these cell tracks while ignoring the time dimension we practically reconstruct the T-r_e plots of the areas in Fig. 3. Because we track the growing cloud elements the reconstruction is closest to the 15 percentile of the T-r_e distribution, shown in Fig. 4.

5. Conclusions

The unique MSG rapid scan data enables us to track the microphysical evolution of the tops of individual convective cloud elements in different areas. It has been shown here that individual clouds follow the general pattern of the T-r_e plot that characterizes the convective cloud cluster in its' specific area, although the individual clouds may be very different dynamically. The single clouds, each in its stage: young, mature or dissipating, join to build the T-r_e plot of the cluster. We showed that the rate and

ACPD
5, 11911–11928, 2005

duration of processes such as diffusional growth and duration of supercooled phase could be inferred from the time sequence, but their variation in duration has little effect on the dependence of r_e on T. The result is that T-r_e relations of a convective cloud field is stable over time, and depends mainly on the thermodynamic and aerosol properties of the air mass. For example, the diurnal increase of instability is associated with a small decrease of the r_e for a given T in the afternoon hours. This is in fact a validation of the ergodicity assumption for the T-r_e relations for a cloud field under given similar conditions.

The validity of the ergodicity assumption is at the basis of the inference of vertical microphysical evolution of convective cloud elements, using a snap shot of convective cloud field (Rosenfeld and Lensky, 1998). This is important because of the much greater resolution of polar satellites that can take only snap shots. The validation of the ergodicity assumption provides a more solid basis for using these satellites snap shots for inferring the microphysical evolution of growing convective cloud elements.

Acknowledgements. The authors thank EUMETSAT for providing the unique MSG rapid scan data set that made this study possible. This study was partially supported by the Israel Space Agency.

References

Freud, E., Rosenfeld, D., Andreae, M. O., Costa, A. A., and Artaxo, P.: Robust relations between CCN and the vertical evolution of cloud drop size distribution in deep convective clouds, Atmos. Chem. Phys. Discuss., 5, 10 155–10 195, 2005, SRef-ID: 1680-7375/acpd/2005-5-10155.

Lensky, M. I. and Rosenfeld, D.: Estimation of precipitation area and rain intensity based on the microphysical properties retrieved from NOAA AVHRR data, J. Appl. Meteor., 36, 234–242, 1997.

Nakajima, T. and King, M. D.: Asymptotic theory for optically thick layers, Appl. Opt., 31, 7669–7683, 1992.

Nakajima, T. Y. and Nakajima, T.: Wide-area determination of cloud microphysical properties from NOAA AVHRR measurements for FIRE and ASTEX regions, J. Atmos. Sci., 52, 4043–4059, 1995.
Ramanathan, V., Crutzen, P. J., Kiehl, J. T., and Rosenfeld, D.: Aerosols, Climate and the Hydrological Cycle, Science, 294, 2119–2124, 2001.
Rosenfeld, D. and Lensky, I. M.: Satellite-based insights into precipitation formation processes in continental and maritime convective clouds, Bull. Amer. Meteor. Soc., 79, 2457–2476, 1998.
Rosenfeld, D.: TRMM observed first direct evidence of smoke from forest fires inhibiting rainfall, Geophys. Res. Lett., 26, 3105–3108, 1999.
Rosenfeld, D: Suppression of rain and snow by urban and industrial air pollution, Science, 287, 1793–1796, 2000.
Rosenfeld, D., Rudich, Y., and Lahav, R.: Desert dust suppressing: A possible desertification feedback loop, Proc. Natl. Acad. Sci. USA, 98, 5975–5980, 2001.
Rosenfeld, D. and Woodley, W. L.: Cloud microphysical observations relevance to the Texas cold-cloud conceptual seeding model, J. Wea. Mod., 29, 56–68, 1997.
Rosenfeld, D. and Woodley, W. L.: Pollution and Clouds. Physics World, Institute of Physics Publishing LTD, Dirac House, Temple Back, Bristol BS1 6BE, UK, February 2001, 33–37, 2001.
Rosenfeld, D., Lahav, R., Khain, A. P., and Pinsky, M.: The role of sea-spray in cleansing air pollution over ocean via cloud processes, Science, 297, 1667–1670, 2002.
Rosenfeld, D. and Woodley, W. L.: Closing the 50-year circle: From cloud seeding to space and back to climate change through precipitation physics, Chapter 6 of "Cloud Systems, Hurricanes, and the Tropical Rainfall Measuring Mission (TRMM)", edited by: Tao, W.-K. and Adler, R., 234 pp., p. 59–80, Meteorological Monographs 51, AMS, 2003.
Rosenfeld, D., Cattani, E., Melani, S., and Levizzani, V.: Considerations on daylight operation of 1.6 μm vs 3.7 μm channel on NOAA and METOP Satellites, Bull. Amer. Meteor. Soc., 85, 873–881, 2004.
Rudich, Y., Rosenfeld, D., and Khersonsky, O.: Treating clouds with a grain of salt, Geophys. Res. Lett., 29(22), doi:10.1029/2002GL016055, 2002.
Rudich, Y., Sagi, A., and Rosenfeld, D.: Influence of the Kuwait oil fires plume (1991) on the microphysical development of clouds, J. Geophys. Res., 108(D15), 4478, doi:10.1029/2003JD003472, 2003.

ACPD
5, 11911–11928, 2005

Schmetz, J., Pili, P., Tjemkes, S., Just, D., Kerkmann, J., Rota, S., and Ratier, A.: An Introduction to Meteosat Second Generation (MSG), Bull. Amer. Meteor. Soc., 83, 977–992, 2002.

Tupper, A., Oswalt, J. S., and Rosenfeld, D.: Satellite and radar analysis of the 'volcanic' thunderstorms at Mt Pinatubo, Philippines, 1991, J. Geophys. Res., 110, D09204, doi:10.1029/2004JD005499, 2004.

Williams, E., Rosenfeld, D., and Madden, M.: Contrasting convective regimes over the Amazon: Implications for cloud electrification, J. Geophys. Res., 107(D20), 8082, doi:10.1029/2001JD000380, 2002.

Woodley, W. L., Rosenfeld, D., and Strautins, A.: Identification of a seeding signature in Texas using multi-spectral satellite imagery, J. Wea. Mod., 32, 37–52, 2000.

ACPD

5, 11911–11928, 2005

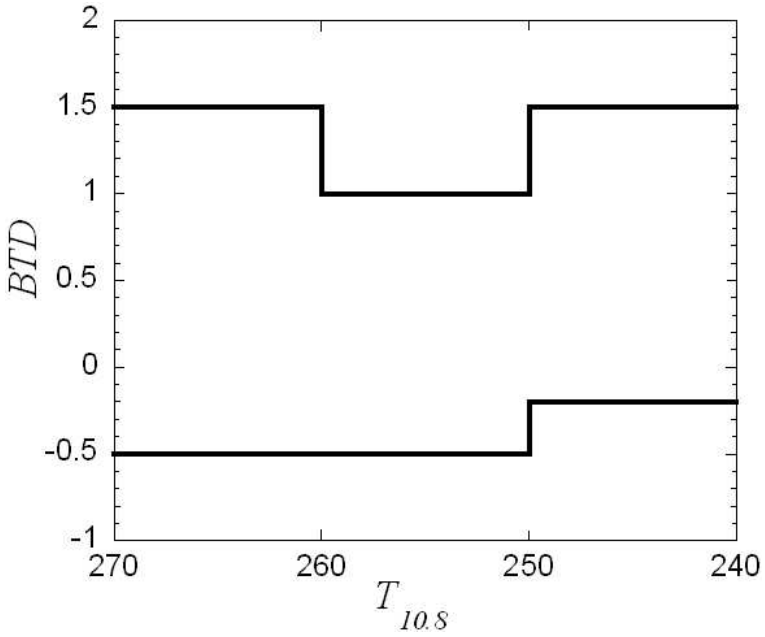

Fig. 1. Temperature dependence of the BTD between 10.8 and 12.0 μm channels thresholds for the cloud mask.

ACPD

5, 11911–11928, 2005

Ergodicity of the T-r_e relations for convective clouds

I. M. Lensky and
D. Rosenfeld

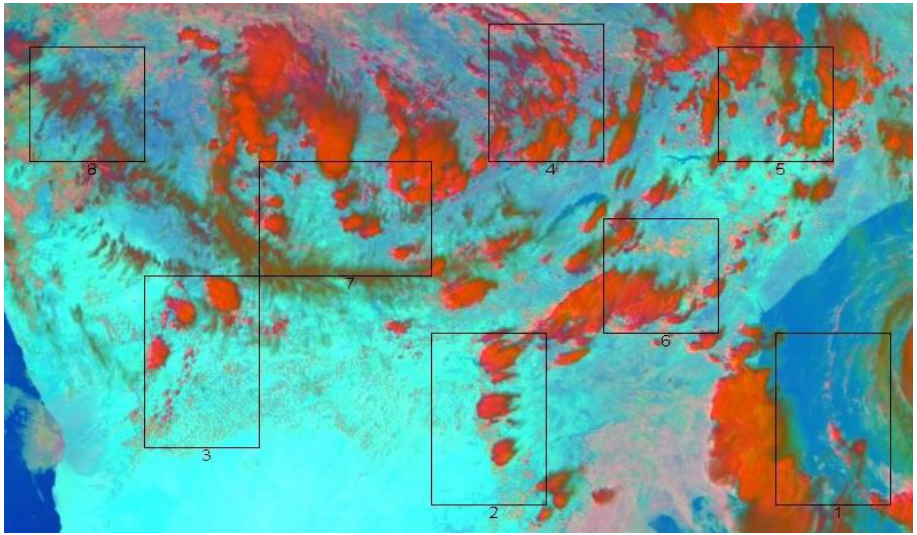

Fig. 2. MSG/SEVIRI image from 15 December 2003 13:01 GMT of convective clouds over southern Africa is shown. The color is composed of red for 0.8 μm reflectance, green for 3.9 μm reflectance (approximating r_e), and blue for 10.8 μm brightness temperature. The selected areas of interest for the analysis of the timespace exchangeability of the T-r_e are shown.

ACPD

5, 11911–11928, 2005

Ergodicity of the T-r_e relations for convective clouds

I. M. Lensky and
D. Rosenfeld

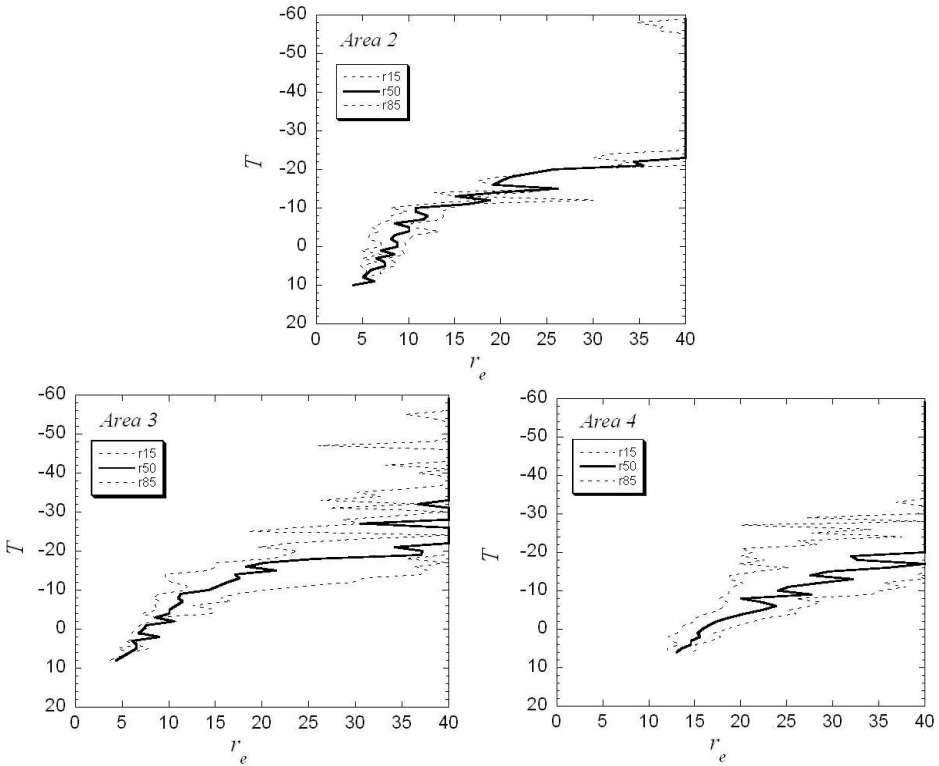

Fig. 3. Analysis of the T-r_e relationship, for all the pixels that passed the cloud mask in areas 2, 3 and 4 from 13:01 GMT. Plotted are the 15th 50th, and 85th percentiles of the re for each 1˚C interval. The thick line indicates the median. Areas 2 and 3 are microphysicaly continental, while area 4 is microphysicaly maritime.

ACPD
5, 11911–11928, 2005

Ergodicity of the T-r_e relations for convective clouds

I. M. Lensky and
D. Rosenfeld

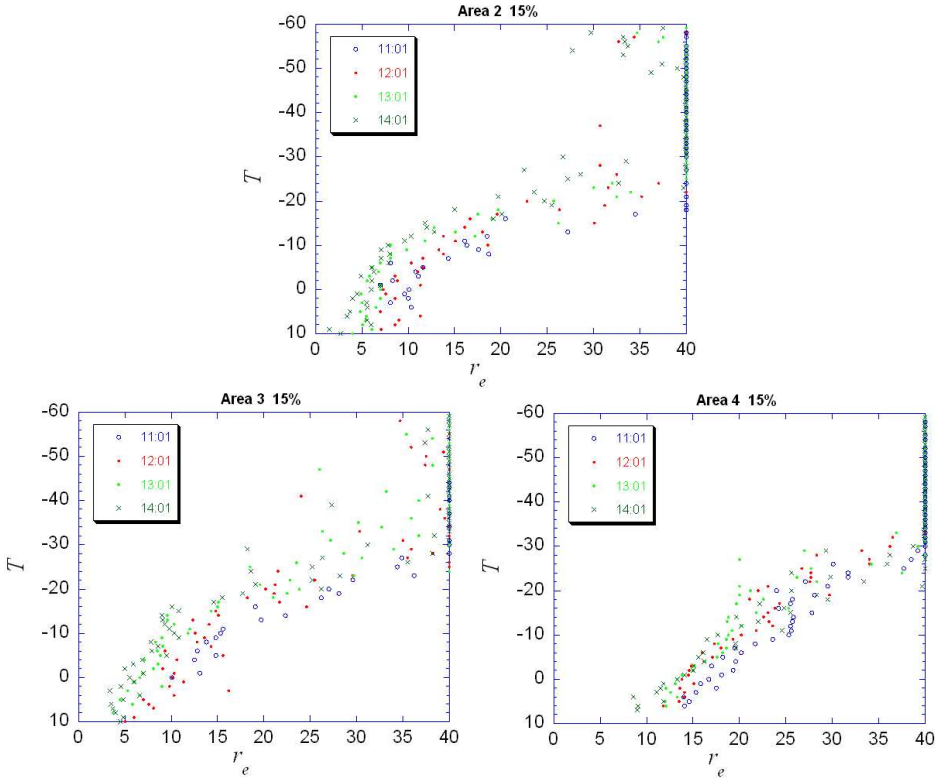

Fig. 4. Same as Fig. 3, but for the 15th percentiles at one-hour intervals: 11:00, 12:00, 13:00 and 14:00 GMT.

ACPD

5, 11911–11928, 2005

Ergodicity of the T-r_e relations for convective clouds

I. M. Lensky and
D. Rosenfeld

EGU

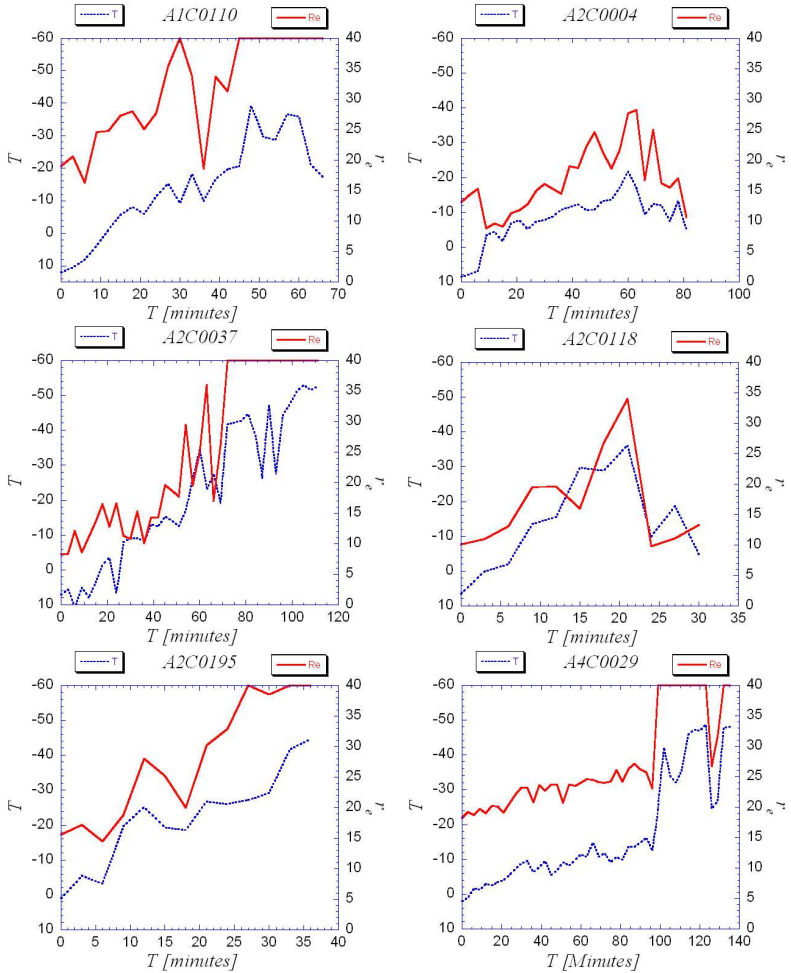

Fig. 5. Time evolution of T and r_e of the cells' coldest pixel of some of the longer tracked convective cells in areas 1, 2 and 4.

ACPD
5, 11911–11928, 2005

Ergodicity of the T-r_e relations for convective clouds

I. M. Lensky and
D. Rosenfeld

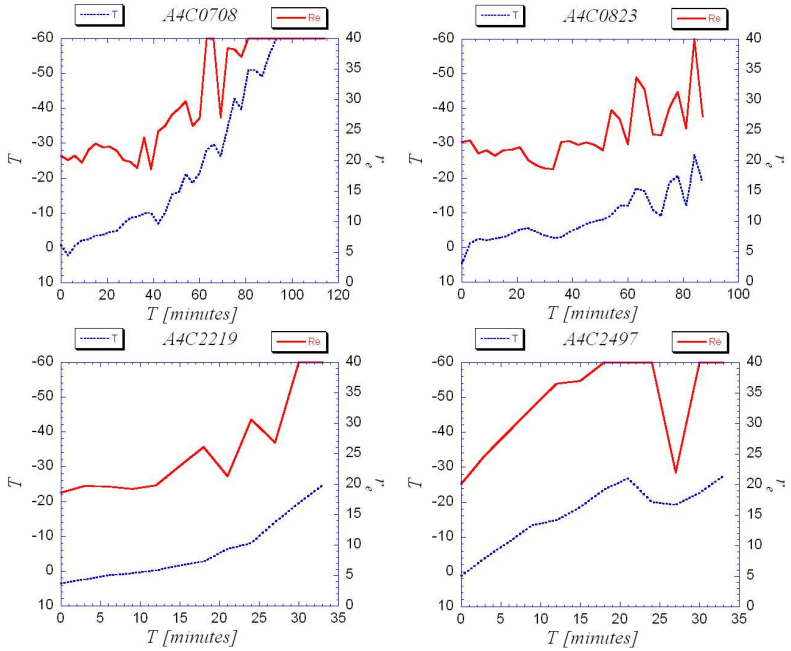

Fig. 5. Continued.

ACPD
5, 11911–11928, 2005

Ergodicity of the T-r_e relations for convective clouds

I. M. Lensky and
D. Rosenfeld

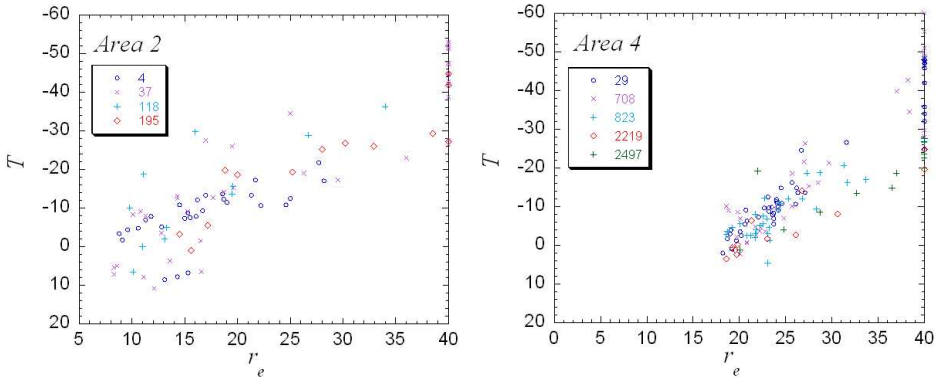

Fig. 6. Scatter gram of the T-r_e of the coldest pixel in the convective cells in areas 2 and 4 that are shown in Fig. 5.

ACPD
5, 11911–11928, 2005

Ergodicity of the T-r_e relations for convective clouds

I. M. Lensky and
D. Rosenfeld